# DC-Bias Dependent Impedance and UV-Vis Diffuse Reflectance Spectroscopy of The Un-Doped and Nb-Doped Ba0.97La0.02TiO3 Ceramics

**Marwa Jebli** ( marwaa.jebli12@gmail.com )
Universite de Monastir Faculte des Sciences de Monastir
**Nejeh Hamadoui**
University of Sousse: Universite de Sousse
**chaker rayssi**
Universite de Monastir Faculte des Sciences de Monastir
**Jemai Dhahri**
Universite de Monastir Faculte des Sciences de Monastir
**Mouna Ben Henda**
Majmaah University
**Nadia Zaidi**
Al Jouf University: Al-Jouf University

**Research Article**

**Keywords:** Electrical properties, Molten-salt, Impedance spectroscopy, Electrochemical Impedance Spectroscopy (EIS) spectra analyzer, Optical properties

**Posted Date:** February 25th, 2021

**DOI:** https://doi.org/10.21203/rs.3.rs-228887/v1

# DC-bias dependent impedance and UV-Vis diffuse reflectance spectroscopy of the un-doped and Nb-doped $Ba_{0.97}La_{0.02}TiO_3$ ceramics

**Marwa Jebli [1,*], Nejeh Hamadoui[2,3], Ch. Rayssi [1], J. Dhahri[1], M. Ben Henda[4] and Nadia Zaidi[5].**

[1] Laboratoire de la Matière Condensée et des Nanosciences, Département de Physique, Faculté des Sciences de Monastir, Avenue de l'environnement, 5019 Monastir, Tunisia.

[2] Laboratoire des Energies et des Matériaux, LabEM-LR11ES34, Ecole Supérieure des Sciences et de la Technologie, University of Sousse, Road Lamine Abessi, Hammam Sousse, 4011 Sousse, Tunisia

[3] Institut Superieur des Technologies de l'Informatique et de la Communication, Gp1, University of Sousse, Hammam Sousse, 4011 Sousse, Tunisia

[4] Department of Physics, College of Sciences at Zulfi, Majmaah University, Zulfi 11932, Saudi Arabia, Saudi Arabia

[5] Physics Department, Faculty of Science, Jouf University, P.O.Box: 2014, Sakaka, Aljouf, Saudi Arabia

***Abstract***

This report typically discusses the Voltage-Stability (V-S) of the electrical properties of a new perovskite oxide, $Ba_{0.97}La_{0.02}Ti_{1-x}Nb_{4x/5}O_3$ (noted BLT, $BLT_{0.9}Nb_{0.08}$) ceramics which have been meticulously studied. The ceramics typically exhibited a low rise in the real and imaginary parts of the complex impedance on the application of small field levels (up to 5 V). These accurate data, at a low voltage threshold, properly designate a hole-generation process which becomes active. These values considered using AC impedance spectroscopy, nonetheless, were relatively decreased with increasing Nb concentration, as well as increased by this application of a DC bias. For each sample, the complex impedance plot displayed a single impedance semicircle, identified over the high and low frequencies. The equivalent circuit configuration was typically fitted using the Electrochemical Impedance Spectroscopy (EIS) spectra analyzer. Importantly, the electrical properties of our both compounds deduced from the complex electric modulus show a conduction process due to the short-range mobility of charge carriers. An excellent addition of Niobium to some considerable extent can inhibit the grain growth. Conspicuously, the substitution of $Nb^{5+}$ ions for $Ti^{4+}$ on B sites leads to the noticeable increase of a band gap. These findings supplied critical insights into the electric mechanisms in BT-based ceramics.

***Keywords:*** Electrical properties, Molten-salt, Impedance spectroscopy, Electrochemical Impedance Spectroscopy (EIS) spectra analyzer, Optical properties.

* **Corresponding author:** Marwa Jebli
**E-mail address:** marwaa.jebli12@gmail.com

## *I. Introduction*

Barium titanate (abbreviated as $BaTiO_3$ or BT) has been the subject of intense research for more than six decades. It is one of the excellent ferroelectric materials with the $ABO_3$ perovskite structure, and it remains the basis of the industry today. [1] It is indeed a frequently used material typically having a dielectric, electrical, optical, piezoelectric and ferroelectric nature. Successful applications of the BT material include its use in thermistors, capacitors, optical devices, and in the electronics industry.

The microstructure, dielectric, and electrical properties of BT can be modified by an enormous variety of substitutions possible at $Ba^{2+}$ on A-sites or $Ti^{4+}$ on B-sides simultaneously or autonomously in perovskite organization. These possible substitutions can be isovalent or heterovalent. The possible effects of isovalent substitutions like $Ca^{2+}$, $Sr^{2+}$, and $Pb^{2+}$ for $Ba^{2+}$ on A-locations and $Hf^{4+}$, $Zr^{4+}$ for $Ti^{4+}$ on B-locations on electric, dielectric, and optical properties of used Barium Titanate ceramics have been thoughtfully examined. Heterovalent substitutions such as $Nb^{5+}$, $Yb^{3+}$, $Er^{3+}$, $Eu^{3+}$, $Nd^{3+}$, $Gd^{3+}$, $Dy^{3+}$, $Sm^{3+}$, $Ho^{3+}$, $Tb^{3+}$, $La^{3+}$, $Bi^{3+}$, $Mg^{2+}$, and so on for $Ba^{2+}$ or $Ti^{4+}$ cause a difference in charge and the possible creation of vacancies on A- or B- site or generation of holes to generally maintain the neutrality of the electric charge. [2-6]

Rare-earth (RE) oxides are popularly known to be useful dopants for ceramic dielectrics due to their functions of stabilizing the temperature-Voltage dependence of dielectric constant and lowering the dissipation factor. Extensive works on the RE ion doped in the BT-based dielectric, electric, and optical. It has been carried out, such as crystal defect chemistry of RE-cations in BT.[7-9] Significantly, rare-earths “RE” dopants are one of the most notable substitutions, for instance; Lanthanide doped $BaTiO_3$ is of considerable importance to the modern electronics industry. [10-11]

In addition, $La^{3+}$ ions can typically decrease the dielectric loss of barium titanate ceramics; moreover, niobium can properly curb the growth of the grains of the barium titanate ceramic and lead to a considerable drop in the Curie temperature. There is an effective diffuse phase transition in barium titanate ceramics doped with $Nb^{5+}$ and $La^{3+}$. [12-16]

Impedance spectroscopy generally represents a versatile tool to adequately characterize the electrical properties of materials, in particular the notable influences of interfaces on the

electrical properties of selected samples [17] for instance; it has been applied to decide the impacts of the limits of grain on the phenomena of polarization of ceramic materials. [18-19] In the doped models, the dopants can be appropriately present as solute particles in the grains, segregate toward the grain limits, or structure the inter-metallic compounds when they surpass as far as possible. This right away changes the carrier transports both in grains and grain limits of the sample and with relieve of the equivalent circuit models, their impacts on conduction behaviors can be esteemed via the impedance measurement at a several frequency.[20-24] Although there are numerous reports of AC impedance spectroscopy on BT-based ceramics, concentrates, including the impacts of DC bias, are relatively rare. [25,26] In other hand, Pure BT is sensibly expected to be highly insulating because of its enormous band gap, be that as it may, restricted measures of contamination dopants can definitely influence its electrical properties. [24] Accurate determination of a material's optical band gap ($E_g$) is critical in predicting relevance and execution in optoelectronic gadgets. The most extensively used strategies for Eg measurement generally involve spectroscopic methods dependent on absorption, for instance, transmission estimations on thin films [27-29] or diffuse reflectance (DR) proceedings on bulk specimens. [30] These predominant strategies are suggested for the estimation of massive properties for the clear explanation that they avoid confounding of bulk properties with surface impacts, attributable to the enormous infiltration profundities of photons in the energy sequence of mostly band gaps of the semiconductors. Higher-energy photoelectron spectroscopy estimations are deliberately restricted by the mean inelastic freeways of the moderately short photoelectrons. They are on the request of a few nanometers, and lead to the drop in the Curie temperature. [30, 31]

In the present work, we typically focus on $Ba_{0.097}La_{0.02}Ti_{1-x}Nb_{4x/5}O_3$ (for x = 0 and 0.1) ceramics compounds, to study the phase purity using the XRD. Furthermore, we articulate the effect of a slight DC bias [0V - 5V] on the electrical has been examined for our stoichiometric solid solutions of Nb-doped $Ba_{0.97}La_{0.02}Ti_{1-x}O_3$ (for x = 0 and 0.1) compositions. A small increase in the real and imaginary parts of the impedance will be shown when applying small field levels (up to 5V). At a low voltage threshold, this observation data correctly points to a hole-generation mechanism that becomes active. In remarkable contrast, these values calculated using AC impedance spectroscopy, however, were relatively decreased with increasing Nb concentration, as well as by the application of DC bias. This precisely represents a significant result from the point of view of electrical mechanisms in BT-based ceramics. It also helps to establish a relationship between traditional DC measurements

implemented to study electrical properties and AC impedance spectroscopy techniques. When determining the values of the optical band gap, by the traditionally direct optical band gap of semiconductors, it is necessary to adequately take into account.

## *II. Experimental procedures*

### *1. Materials and sample synthesis*

A set of $Ba_{0.97}La_{0.02}Ti_{1-x}Nb_{4x/5}O_3$ (for x = 0 and 0.1) perovskite ceramics were synthesized by high temperature molten-salt reaction method. As indicated by the specific stoichiometric ratio the high purity Barium carbonate (($BaCO_3$), 99%), Titanium oxide (($TiO_2$), 99.9%), Lanthanum acetate (($LaCH_3CO_2$), 99.9%) and Niobium chloride (($NbCl_5$), 99%) as the starting crude materials. The stoichiometric amount of $BaCO_3$, $TiO_2$, $NbCl_5$ and ($LaCH_3CO_2$) were taken and altogether blended for 2h in agate mortar employing 1:10 eutectic KCl to acquire the homogeneous compound. At that point, the blend was gathered and transferred into an alumina crucible followed by the calcinations in a furnace at 800 °C for 24 hours. After that, with distilled water, these mixes were washed. Then they filtered to eliminate the salts, and the residue was dried at 100 °C in air. This cycle was rehashed multiple times to accomplish homogeneous and nano-polycrystalline powders. After grinding thoroughly, the powders were squeezed into circular pellets of a few millimeters thick (~2 mm) and a diameter of 8 mm. The obtained pellets were conveniently located into alumina crucible and sintered in air at 800°C for 24h.

### *2. Sample characterization technique*

To investigate the crystal structure and phase of $Ba_{0.97}La_{0.02}Ti_{1-x}Nb_{4x/5}O_3$ (x = 0 and 0.1), the XRD (X-ray diffractometer) were typically performed. The XRD of prepared samples were accounted in a wide scope of Bragg angles 2θ ($10° \leq 2\theta \leq 90°$) with a 0.02° step size and a utilizing recorded on a PANalytical X'Pert Pro diffractometer with Cu-Kα radiation (λ = 1.54060Å). After cathodic sputtering of the gold electrodes on the circular faces, the dielectric properties were expressed from the ceramic discs. The Voltage-dependent at various frequencies electrical measurements on the pellets were performed with an impedance analyzer (4NLPSM1735), an over large sequence of frequencies from 100Hz to 5MHz. The UV-Vis diffuse reflectance spectra were recorded with the help of "Perkin Elmer Lambda 35 UVVis-NIR Spectrophotometer in the wavelength range 200 to 800 nm. All measurements were performed at room temperature.

## *III. Results and discussion*

### *1. Crystal structural:*

Compounds of $Ba_{0.97}La_{0.02}Ti_{1-x}Nb_{4x/5}O_3$ (x = 0 and 0.1) ceramics appeared to be effectively single-phase by XRD; there was no proof of any auxiliary phases in our compositions. (See **Figure.1**) Their consistent patterns closely resembled those of tetragonal perovskite for the tow samples, space group **P4/mmm** and were indexed accordingly with refined lattice parameters summed up in **Table.1**: lattice parameters, especially c and the unit cell volume, demonstrate a small decrease with x; it very well may be clarified by the rayon ionic radii $Nb^{5+}$ substitutes for $Ti^{4+}$. [32,33]

## *2. Electrical properties*

### *2.1. Impedance spectral analysis*

The perovskite properties have influenced for a several factors, such as, the morphology of the surface, their thickness, the mismatch of the lattice, the structure of the interface between the sub-layers, character of the constituent materials, etc. As a general rule, it relies upon the role that interfaces and electrodes play, and the way they influence its behavior. At the interface, the physical properties, crystallographic, mechanical, compositional, and, specifically, electrical response, change precipitously, and heterogeneous charge distributions (polarizations) progressively reduce the overall electrical conductivity during a framework. Conventionally, complex impedance spectroscopy (CIS), [34] is without a doubt a ground-breaking trial technique to separate and study the electrical route in a framework, which occurs between electro-dynamic districts and their interfaces when it applies a discontinuous signal at aggravation input. Between intrinsic (bulk or grain) and extrinsic (grain boundary, surface layer and electrode) contributions, the output signal makes it possible to recognize it.

As a function of electrical properties, the ac impedance method permits a complete interpretation of the frequency-temperature with or without application of DC-bias has been examined [35].

The data information can be deliberately analyzed as far as four possible complex formalisms, such as, the impedance ($Z^*$), admittance ($Y^*$), electrical modulus ($M^*$), and relative permittivity $\varepsilon^*$, which are associated concerning each other according to **Table.II**.

A sinusoidal signal of low amplitude is applied across a sample, in the impedance spectroscopy technique. The phase shift ($\theta$) and impedance ($Z^*$) are measured straightforwardly at the output. In the complex plane, the exposure to view of the impedance information is presented as a succession of semicircles attributed to relaxation phenomena with enough different time constants to allow the separation of each contribution: [36-39]

(i) The high frequency area is attributable to the phenomenon of grains.

(ii) Intermediate frequency due to the aspect of the grain limit.

(iii) The low frequency region is due to the material-electrode interface event. This strategy has also been applied to explore the electrical-microstructure relationship of several multiferroic composites.

The real (′) and imaginary (″) components of complex impedance quantities (*) and the related parameters of the materials have been viewed as utilizing the essential conditions [35] can be demonstrated in the **Table.II**, where, the parameters ($C_0$, $C_s$, and $R_s$), represents, respectively, the vacuum capacitance, series capacitance, and series resistance.

Nyquist plots of BLT and $BLT_{0.9}Nb_{0.08}$ ceramics under different DC-bias, shown in **Figure.2**. As this figure, there is an obvious sign of semicircle in the high-frequency region. The Cole-Cole graph at medium and high frequencies is depicted by the dominance of a large overlapping semi-arc. However, the large semi-arc can further separate into two electrical elements associated with grain boundary response at mid-frequency.

The Nyquist values of BLT and $BLT_{0.9}Nb_{0.08}$, furthermore, containing ceramics increased when applying a low DC-bias voltage. What's importantly, there was a slight increase in resistivity values. [24] These two phenomena were reversible, that is, the resistivity returned to its unbiased values shortly after the DC-bias was removed. [24] $BLTi_{1-x}Nb_{4x/5}O_3$ (x = 0, 0.1) ceramic impedance information data can be effectively modeled using an equivalent electrical circuit consisting of an equivalent circuit. This circuit contains two parallel elements (R//CPE): (R-resistance, CRE-constant phase element), as appeared in the inset of figure 5, where ($R_g$//$CPE_g$) and ($R_{gb}$//$CPE_{gb}$) depict the grains, and an obscure electrical boundary, respectively. (See **Figure.2**)

The evolution of the real part of the impedance (Z′) as a function of the frequency in the interval [1-$10^7$ Hz] at different DC-bias voltage for BLT and $BLT_{0.9}Nb_{0.08}$, respectively, is displayed in **Figure.3**. [40]

We have examined that Z′ decreases gradually with rising frequency as well as the DC bias voltage. Also, at low frequencies, Z′ has the most elevated value. Afterward, for BLT and $BLT_{0.9}Nb_{0.08}$, it becomes constant (independent of frequency) as well as the application of a low DC-bias voltage and merges at a high frequency. This outcome is due to the release of the polarization of the space charge in the material. [41] For a given frequency, the value of Z′ diminishes with an increase in the amount of the Niobium. (See **Figure.3**)

This behavior attributed to the increased in space-charge accumulation at grain boundaries.

At the DC bias voltage, the evolution of the imaginary part of the complex impedance (Z″) as function of frequency, with various concentrations of Nb, illustrated in **Figure.4**. This figure is distinguished by:

(i) For BLT and $BLT_{0.9}Nb_{0.08,}$ the curves demonstrate that the Z″ values achieve a maximum peak ($Z''_{max}$), at a selected frequency is understood because the frequency of electrical relaxation ($f_{max}$).

(ii) We can notice a typical peak broadening, slightly asymmetric in nature.

(iii) With increasing concentrations of Nb, the value of $Z''_{max}$ shifts to higher frequencies.

The merger of Z″ could be the sign of the being of a relaxation of space charge, in the region of the high frequencies. The polarization of the spatial charge is dominant when the material is composed of grains and grain boundaries. [42-44] Also, the decrease of Z″ is clarified by the decrease in the resistive part of the samples.

### *2.2.Electrical modulus analysis*

Analysis of the electrical module is an important process. It is interesting to distinguish the polarization of the electrodes, the conduction effect at the grain boundaries, the bulk properties, the electrical conductivity and the relaxation time. [45] At various frequencies, this technique additionally provides knowledge about the electrical processes occurring in the materials. [46] Physically, the complex modulus formalism is an important and advantageous gadget for dissecting and deciphering the dynamic aspects of electrical transport phenomena, i.e. parameters such as carrier/particle hopping rate, relaxation time conductivity, etc. It gives knowledge about electrical processes characterized by the smallest capacity of materials. In addition, the following electrical module relations can be used to assess M 'and M ″ based on the real and imaginary part of the impedance: [47]

$M^{'} = \omega C_0 Z^{''}$ : The real part of modulus. (1)

$M^{''} = \omega C_0 Z^{'}$ : The imaginary part of modulus. (2)

In the material, the physical meaning of the electric modulus is the mechanism of relaxation of the electric field, as the electric displacement remains constant. The frequency dependent characteristics of M′ and M″ are wonderful methods for studying the relaxation process. [48]

At various DC bias voltages, the frequency dependence of the real part of the dielectric modulus (M′), for BLT and $BLT_{0.9}Nb_{0.08}$, has been verified in **Figure.5**. It has a low value (close to zero). This outcome indicates that the phenomena effects of the electrode are ignored. [49] In addition, with the increase in frequency and the low DC bias voltage, the values of M′ augmented and demonstrated a dispersion tending towards $M_\infty$ (the asymptotic value of M′ at higher frequencies). At lower value of frequencies, M′ was very low (very close to zero) at lower frequencies, [50] and tended to increase with increasing frequency and DC bias voltage. By increasing the DC bias voltage as well as the frequency, this variation

was indicated as continuous dispersion. This dispersion may be a direct consequence of conduction phenomena due to the short-range mobility of charge carriers under the action of an induced electric field. [51-52] The Kind of evolution has indicated that the electrical properties of materials are due to volume (intra-grain). This implies the absence of a restoring force for the flow of charge under the effect of a constant electric field.

At a small voltage of varied DC bias, the variation of the imaginary part of the electric module (M") of $Ba_{0.97}La_{0.02}Ti_{1-x}Nb_{4x/5}O_3$ (x = 0, and 0.1) with the frequency appeared in **Figure.6**. This curve is differentiated by a single relaxation peak occurring at a particular frequency and the beginning of increases of a second peak at higher frequency ranges. We can also view that the amplitude of the peaks and the position of the peaks have shifted to the high frequency side with the increase in the doping concentration of Niobium.

The evolution of the peak position of the imaginary part of the modulus of our compounds is linked to the distinction of the cationic distribution and of the microstructure. [53] To better understand this phenomenon, when the M″ peak appears on the low frequency side, it represents the range of frequencies in which the charge carriers can travel from one site to the neighboring site over a long distance (i.e. that particles can successfully jump from one site and then to the next (performing long-range mobility) to a specific frequency (maximum frequency). [54] However, if the peak M″ appears on the high frequency side, this indicates that the range of frequencies in which the charge carriers can trap. n this way, the long range to short range displacement transition of the carriers can be found in our investigation with the increase in frequency. [55-57] The broadening of the peak with various time constants indicates the dispersion of the relaxation time, and therefore a non-Debye type of relaxation is seen in the material. [58, 59]

**Figure.7** appears the Cole–Cole plots (M″ versus M′) for BLT and $BLT_{0.9}Nb_{0.08}$ at different DC-bias. The Cole - Cole plot of the module appropriately displays a wide semicircular arc. It qualified for the grain effect (conductive regions). At high frequency, the onset of another arc, what's more, involved the weak response of the grain boundaries (resistive plates). Basically, for the separation of the relaxation effects of grains and grain boundaries in materials, we used the benefit of this study is more viable than the Nyquist plot of the impedance investigation (Z' vs Z"). **Figure.7** shows a single semicircle and the start of the next semicircle recommends the presence of both grain contributions and grain boundaries in our compounds with the grain dominant effect. This is why the grain boundary semicircle is insignificant compared to the grain semicircle. [53] With the huge difference (orders of magnitude) between the resistive values of the grains and the grain boundaries, it is baffling to

get two full semicircles for the grains and the grain boundary on the same scale in the graph of impedance. Examination of the complex modulus is appropriate because the materials fundamentally have comparative strength, albeit a distinctive ability.

## *3. Optical study*

### *3.1 . Optical band gap energy of the undoped and Nb-doped BLT ceramic*

Generally, the method created by Tauc for demining the value of the direct optical band gap of semiconductors has also been widely used. This process evaluates by extrapolating the straight area (linear region) of the square of the absorption curve to the x-axis. The application of the suitable Tauc process to crystalline materials is established in a misconception and traditional linear extrapolation techniques are suitable for use on degenerate semiconductors, where the occupation of the energy states of the conduction band cannot be overlooked. [61]

For semiconductor materials, the energy band gap is an extremely critical parameter in the application of optoelectronics. The energy band gap of $Ba_{0.97}La_{0.02}Ti_{1-x}Nb_{4x/5}O_3$ (x = 0 and 0.1) can be determined using Kubelka-Munk Theory. The generally settled practice in the experimental determination of Eg from bulk samples is to first convert diffuse reflectance "DR" spectra of prepared Niobium into pseudo-absorption spectra F(R) via the Kubelka–Munk function [62] and enunciated as:

$$F(R_\infty)=\frac{K}{S}=\frac{(1-R_\infty)^2}{2R_\infty} \quad (3)$$

Where;

F(R∞): Kubelka-Munk function,

K: absorption coefficient

S: scattering coefficient.

The scattering coefficients of the most materials are comparatively invariant along the visible range of the optical spectrum, that's why S can be treated respectfully as a constant; appropriately, F(R) can be treated as a pseudo-absorption function, and $R\infty = R_{sample}/R_{standard}$, where R is the reflectance of an infinitely thick sample.

In the parabolic band structure, the band gap ($E_g$), and the absorption coefficient α of a direct band gap, for n=1, the semiconductors are originally related through the well referenced to the equation by Tauc [63] as:

$$\alpha h\nu = C(h\nu - Eg)^{\frac{n}{2}} \quad (4)$$

Where,

α: the optical absorption coefficient.

hυ: the energy of the incident photon.

Eg: the determined optical band gap of samples.

C: the energy independent constant.

At the point when the material scatters in a perfectly diffuse manner (or when it is illuminated at 60° incidences.), the K-M absorption coefficient K becomes equal to 2α (K = 2α). In this case, considering the K-M scattering coefficient S as constant with respect to the wavelength, Eq.2 can be adjusted as:

$$F(R_\infty)h\nu = C(h\nu - E_g)^{\frac{n}{2}} \quad (5)$$

Where, all the symbols have their typical meanings.

From the linear extrapolation of $\left[F(R_\infty)h\nu\right]^2 = 0$ exposed in **Figure.8**, the "$E_g$" value was assessed to be about 3.31 and 3.39 for BLT and $BLT_{0.9}Nb_{0.08}$, respectively, due to the diminished average crystallite size. [32, 33] It can be seen that the optical band gap energy increments with Nb rates. [64- 65] These obtained values of "$E_g$" established that the two compounds of polycrystalline ceramic perovskites were all semiconductor materials.[66]

This adjustment in band gap can be clarified by the Burstein-Moss shift: doping increases electrons density in the conduction band and more energy is needed to energize electrons from the valence band to the conduction band.[67]

The band gap of the material is commonly identified with the excitation of the electrons from the highest point of the valence band to the electronic states near the bottom of the conduction band. These outcomes in elevation of the Fermi level into the conduction band of the degenerate semiconductor due to the increase in the carrier density, which brings about the band gap broadening. [68, 69]

## IV. Conclusion:

A simpler, using high temperature at the homogenization step was proposed for the suitable preparation of high-purity $Ba_{0.97}La_{0.02}Ti_{(1-x)}Nb_{4x/5}O_3$ (x = 0 and 0.1) examples. The selected samples were successfully synthesized via molten-salt technique and characterized by X-ray diffraction, electrical properties and UV-Visible methods.

At room-temperature (RT), the structural investigation typically exhibits the presence of a single phase which crystallizes in the tetragonal perovskite crystal structure with *P4/mmm* space group, for our tow examples. We have investigated the effect of doping a material to modify the electrical properties. The real (‘) and imaginary (") parts of complex impedance and modulus properties of the materials were inspected using a complex impedance spectroscopy (CIS) procedure. These latter describe by a strong dependence on frequency. Z´

value is found to diminish with increasing Niobium amount. This reduction is credited to the expansion in space-charge accumulation at grain boundaries. The Nyquist plot (Z" vs. Z') is depicted by the existence of a semi-circular arc at high and a low frequency.

The equivalent circuit was fitted using the Electrochemical Impedance Spectroscopy (EIS) spectra analyzer. This circuit contains a serial association of tow R//CPE(R-resistance, CPE-constant phase element) related in the serial. The electrical properties of our samples demonstrate from the complex electric modulus exhibit a conduction process in view of the short range mobility of charge carriers.

The imaginary (") a part of the complex electric modulus is portrayed by the presence of the height which moved to the high-frequency side with increasing the doping concentration. The variety within the peak position of the imaginary (") a part of the modulus of our examples is identified to the variability with the cation distribution. The electrical properties of our examples assumed from the complex electric modulus prove the existence of a conduction mechanism owing to the short-range mobility of charge carriers. Evenly, Nb-rates increased band gap from 3.31 to 3.39 eV which can be certified to the Burstein-Moss effect.

**Reference:**


1. A. Von Hippel, Rev. Mod. Phys., 22, 221 (1950).
2. Stanciu, C. A., Cernea, M., Secu, E. C., Aldica, G., Ganea, P., & Trusca, R. Journal of Alloys and Compounds, 706, 538-545 (2017).
3. M.T. Biscaglia, V. Buscaglia, M. Viviani, P. Nanni, M. Hanuskova, Journal of European Ceramic Society, 20, 1997–2007 (2000).
4. SINGH, Dhananjay Kumar, MONDAL, Kanchan, and MANAM, J. Ceramics International, 43, 13602-13611 (2017).
5. Vega, M., Fuentes, S., Martín, I. R., & Llanos, J. Materials Research Bulletin, 86, 95-100 (2017).
6. Rubayyat Mahbub, Md. Sazzad Hossain, Md. Fakhrul Islam, Materiálové inžinierstvo (MEMI) Journal, 20, 45- 53 (2013).
7. Badapanda, T., Sarangi, S., Behera, B., Parida, S., Saha, S., Sinha, T. P., ... & Sahoo, P. K. Journal of Alloys and Compounds, 645, 586-596 (2015).
8. LI, Wei, WANG, Zhe, HAO, Jigong, et al., Journal of Materials Chemistry C, 6, 11312-11319 (2018).
9. ALKATHY, Mahmoud S., HEZAM, Abdo, MANOJA, K. S. D., et al./ Journal of Alloys and Compounds, 762, 49-61(2018).
10. Kilbourn, B. T. Inorganica Chimica Acta, 140, 335-338 (1987)..
11. Charalampides, Georgios, et al./ Procedia Economics and Finance 24, 126-135 (2015).
12. B. Wodecka-Dus, D. Czekaj, Archives of Metallurgy and Materials, 54(4), 923-933(2009).
13. T. Dechakupt, J. Tangsritrakul, P. Ketsuwan, R. Yimnirun, Ferroelectrics 415,141-148 (2011).
14. M. Ganguly, S. K. Rout, T. P. Sinha, S. K. Sharma, H. Y. Park, C. W. Ahn and I. W. Kim, Journal of Alloys and Compounds, 579, 473 (2013).
15. F. D. Morrison, D. C. Sinclair and A. R. West, International Journal of Inorganic Materials, 3, 1205 (2001).
16. K. Aliouane, A. Guehria-Laidoudi, A. Simon and J. Ravez, Solid State Sciences, 7, 1324 (2005).
17. J. R. MacDonald, J. Electroanal. Chem. 223, 25 (1987).
18. S. Rodewald, J. Fleig, and J. Maier, J. Am. Ceram. Soc. 84, 521 (2001)
19. J. R. Jurado, M. T. Colomer, and J. R. Frade, J. Am. Ceram. Soc. 83, 2715 (2000)
20. K. El Adham and A. Hammou, Solid State Ionics 9–10, 905 (1983).

21. P. Stallinga, H. L. Gomes, M. Murgia, and K. Mullen, Org. Electron. 3, 43 (2002).
22. P. Stallinga, A. R. V. Benvenho, E. C. P. Smits. S. G. J. Mathijssen, M. Co¨lle, H. L. Gomes, and D. M. de Leeuw, Org. Electron. 9, 735 (2008).
23. Pengrong Ren, Nahum Maso, Yang Liu, Le Ma, Huiqing Fan and Anthony R. West. J. Mater. Chem. C, 1, 2426–2432 (2013).
24. Kumar, N., Patterson, E. A., Frömling, T., & Cann, D. P., Journal of Materials Chemistry C, 4(9), 1782-1786 (2016).
25. Q.-L. Zhang, N. Maso´, Y. Liu, H. Yang and A. R. West, J. Mater. Chem., 21, 12894 (2011).
26. L. Gil Escrig, M. Prades, H. Beltra´n, E. Cordoncillo, N. Maso´ and A. R. West, J. Am. Ceram. Soc., 97, 2815 (2014).
27. F.M. Amanullah, K.J. Pratap, V. Hari Bab, Thin Solid Films 254 (1–2) (1995) 28–32.
28. N.M. Torkaman, Y. Ganjkhanlou, M. Kazemzad, H.H. Dabaghi, M. KeyanpourRad, s, Mater. Charact. 61(3), 362–370 (2010).
29. C.G. Granqvist, A. Hultåker, Thin Solid Films 411 (1), 1–5 (2002).
30. A. Dolgonos, K. Lam, K.R. Poeppelmeier, A.J. Freeman, T.O. Mason, J. Appl. Phys. 115 (1) 013703 (2014).
31. A. Klein, C. Körber, A. Wachau, F. Säuberlich, Y. Gassenbauer, R. Schafranek, S. P. Harvey, T.O. Mason, , Thin Solid Films 518 (4) 1197–1203 (2009).
32. M. Jebli, Ch Rayssi, N. Hamdaoui, S. Rabaoui, J. Dhahri, M. Ben Henda, I. Shaarany, J. Alloys Compd. **784**, 204–212 (2019)
33. Jebli, M., Rayssi, C., Dhahri, J. et al., Appl. Phys. A **126**, 109 (2020)
34. E. Barsoukov and J. R. Macdonald, Impedance Spectroscopy Theory, Experiment and Applications, second ed., (Wiley, New Jersey, 2005).
35. J. ROSS Macdonald. Annals of Biomedical Engineering, 20, 289-305 (1992).
36. C. M. Kanamadi, J. S. Kim, H. K. Yang, B. K. Moon, B. C. Choi, and J. H. Jeong, J. Alloys and Compounds 481, 781 (2009).
37. P. Murugavel, D. Saurel, W. Prellier, Ch. Simon, and B. Raveau, Appl. Phys. Lett. 85, 4424 (2004).
38. J. Wua and J. Wangb, Appl. Phys. Lett. 105, 124107 (2009).
39. S. Maity, D. Bhattacharya, and S. K. Ray, J. Phys. D: Appl. Phys. 44, 095403 (2011).
40. Zhang, Q. L., Masó, N., Liu, Y., Yang, H., & West, A. R., 21(34), 12894-12900 (2011).
41. C.K. Suman, K. Prasad, R.N.P. Choudhary, J. Mater. Sci. 41 (2006) 369.

42. R.V. Mangalaraja, S. Ananthakumar, P. Manohar and F. D. Gnanam, J. Magn. Magn. Mater. 253, 56 (2002).
43. Ch. Rayssi, F. I. H. Rhouma, J. Dhahri, K. Khirouni, M. Zaidi, Hafedh Belmabrouk, Applied Physics A, 123-778 (2017).
44. Monojit Bag, Lawrence A. Renna, Ramesh Y. Adhikari, Supravat Karak, Feng Liu, Paul M. Lahti, Thomas P. Russell, Mark T. Tuominen, and D. Venkataraman, J. Am. Chem. Soc. 137, 13130- 13137 (2015).
45. I.M. HODGE, M.D. INGRAM and A.R. WEST, J. Electroanal. Chem., 74, 125-143 (1976).
46. G. Nag Bhargavi, Ayush Khare, Tanmaya Badapanda, M. Shahid Anwar, Nameeta Brahme, J. Mater. Sci. Mater. Electron. 28, 16956-16964 (2017).
47. M. Kaiser, Mater. Res. Bull. 73 (2016) 452-458.
48. Ch. Rayssi, S. El.Kossi, J. Dhahri and K. Khirouni, RSC Adv. 8, 17139–17150 (2018).
49. A.K. Himanshu, B.K. Choudhary, S.N. Singh, D.C. Gupta, S.K. Bandyopadhayay, T.P. Sinha, Solid State Sci. 12, 1231–1234 (2010).
50. Y.B. Taher, A. Oueslati, K. Khirouni, M. Gargouri, Mater. Res. Bull. 78, 148–157 (2016).
51. S. Nasri, M. Megdiche, M. Gargouri, Physica E Low Dimens. Syst. Nanostruct. 84, 182–190 (2016).
52. Y.B. Taher, A. Oueslati, K. Khirouni, M. Gargouri, J. Clust. Sci. 26, 1655–1669 (2015).
53. Ritu Verma, Surya Prakash Tiwari, Reena Kumari, Ritu Srivastava, J. Mater. Sci. 53, 4199-4208 (2018).
54. K. Majhi, K.B.R. Varma, K.J. Rao, Appl. Phys. 106, 084106 (2009)
55. J. Jadhav, S. Biswas, Ceram. Int. 42, 16598–16610 (2016)
56. K. Prasad, K. Priyanka, K.P. AmarNath, K.P. Chandra, A.R. Kulkarni, J. Mater. Sci. 25, 4856–4866 (2014)
57. Z. Wang, W. Zhou, L. Dong, X. Sui, H. Cai, J. Zuo, Q. Chen, J. Alloys Compd. 682, 738–754 (2016).
58. A. Tabib, N. Sdiri, H. Elhouichet, M. Férid, J. Alloys Compd. 622, 687–694 (2015)
59. L. Singh, U.S. Rai, K. Mandal, B.C. Sin, S.-I. Lee, Y. Lee,. Ceram. Int. 40, 10073–10083 (2014).
60. S.T. Assar, H.F. Abosheiasha, M.K. El Nimr, J. Magn. Magn. Mater. 350, 12-18 (2014).

61. A. Dolgonos et al./ Journal of Solid State Chemistry 240, 43–48 (2016).
62. P. Kubelka, F. Munk, An article on optics of paint layers, Z. Tech. Phys. 12, 593–603 (1931).
63. Singh, D. K., & Manam, J., Electronic Materials Letters, 13(4), 292-301 (2017)..
64. O. Makuku et al./ Ceramics International 42 (2016) 14581–14586
65. L. Wang et al./ Thin Solid Films 517 (2009) 3721–3725
66. W. Haron, A. Wisitsoraat, U. Sirimahachai, and S. Wongnawa, J. Sci. Technol., 40, 484–491 (2018).
67. S.K. Gagandeep, B.S. Lark, H.S. Sahota, Nucl. Sci. Eng. 134, 208–217 (2000).
68. R. Ferro, J.A. Rodriguez, Thin Solid Films 347, 295–298 (1999).
69. A. Davoodi et al./ Optik 127, 4645–4649 (2016).

# Figures

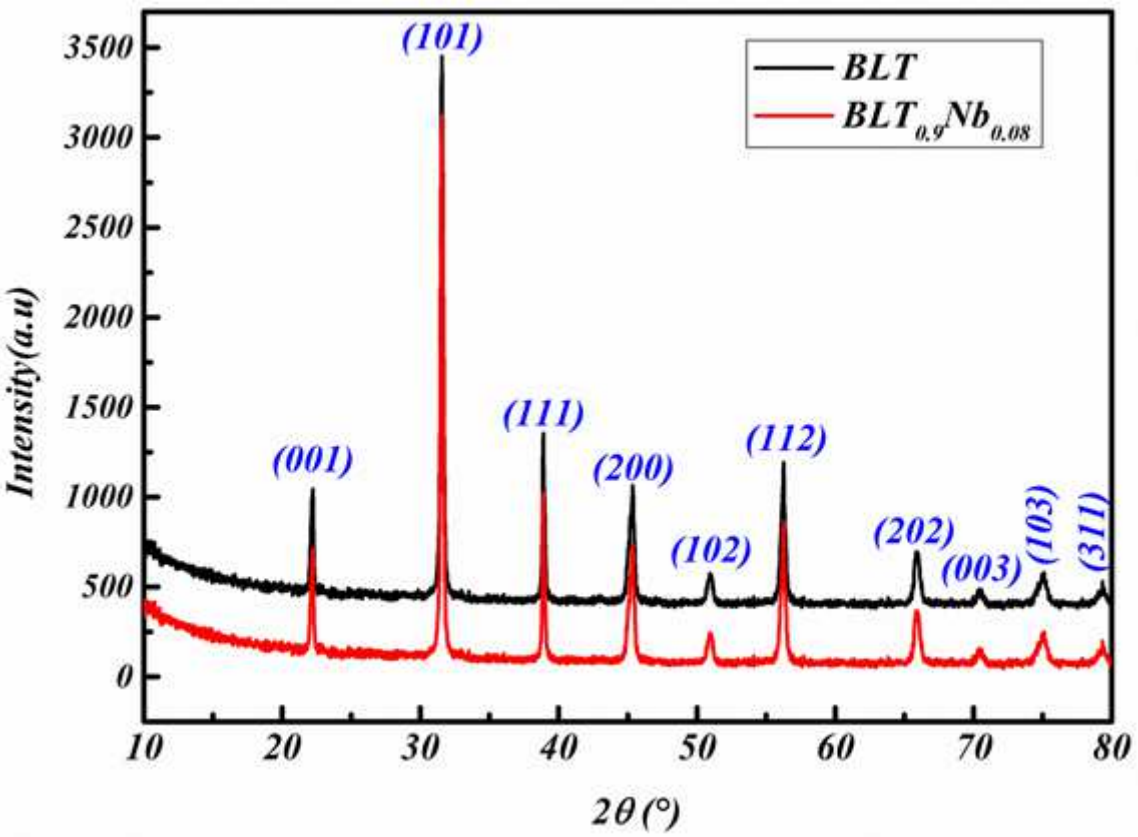


**Figure 1**

XRD patterns of tow samples: (a) BLT ceramic, (b) BLT0.9Nb0.08 ceramic.

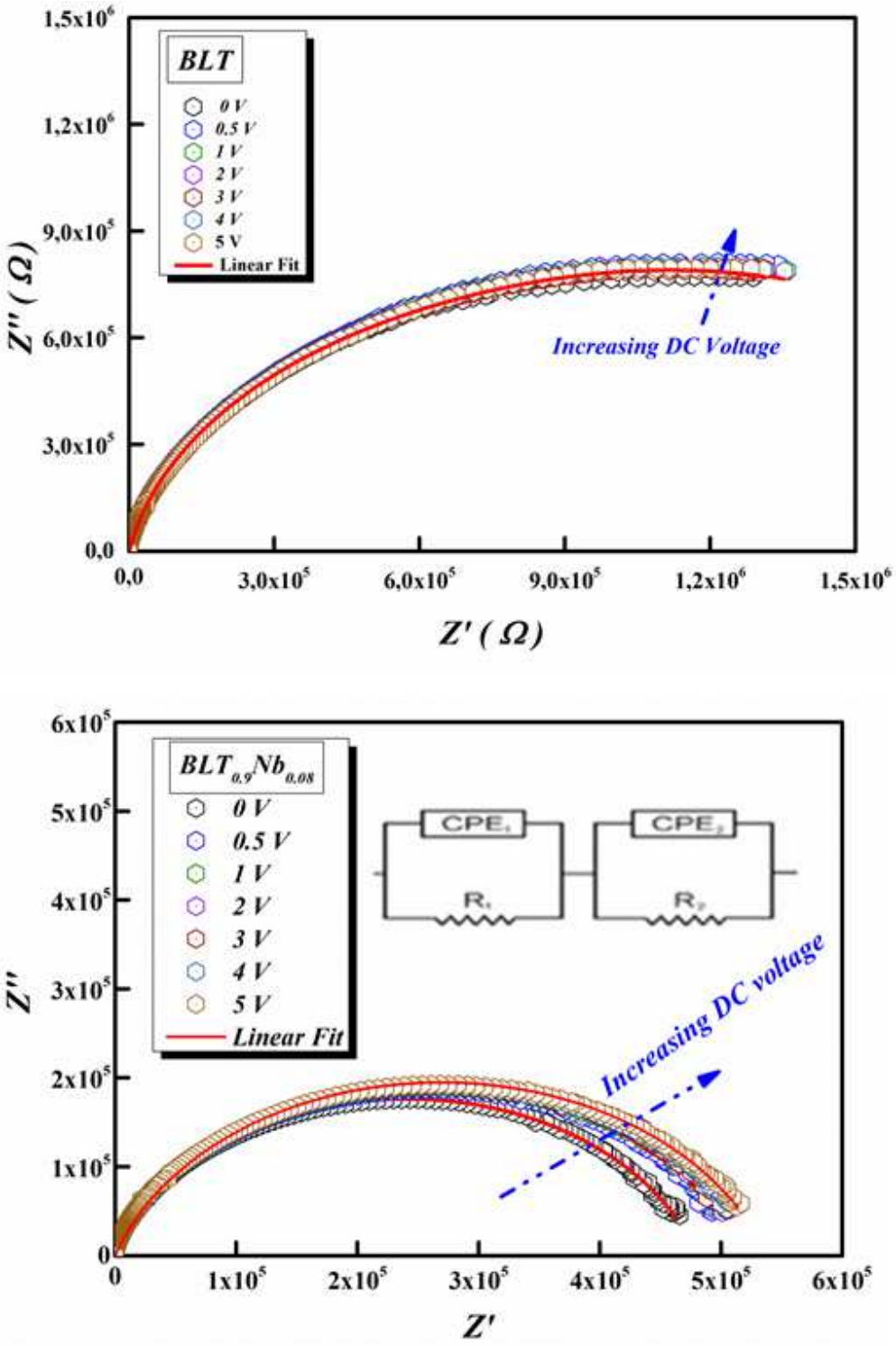


## Figure 2

Complex plane plots with DC bias between [0-5V] for BLT and BLT0.9Nb0.08 ceramic samples.

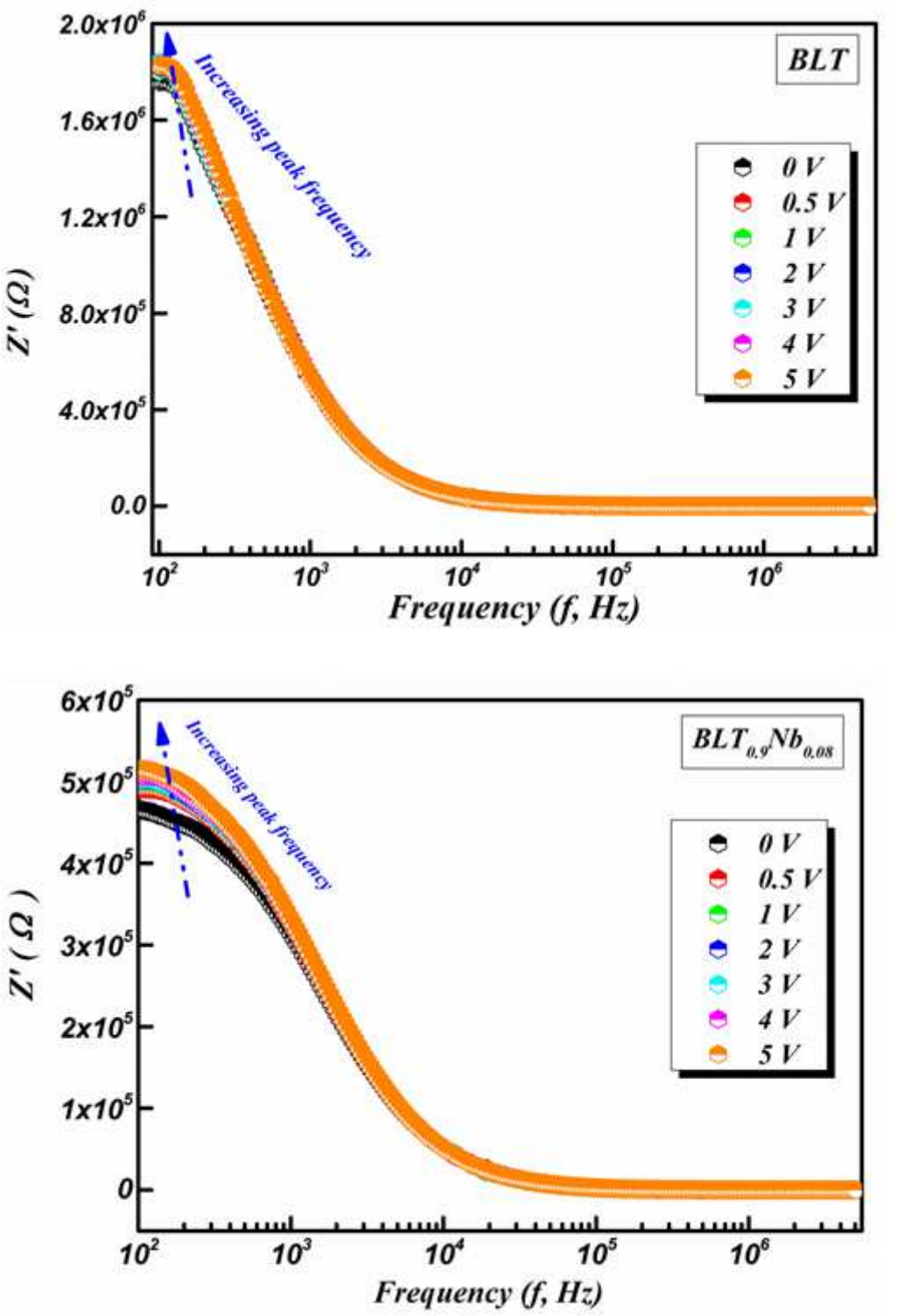


## Figure 3

Real part of impedance as a function of DC-bias (V) for BLT and BLT0.9Nb0.08 ceramic samples.

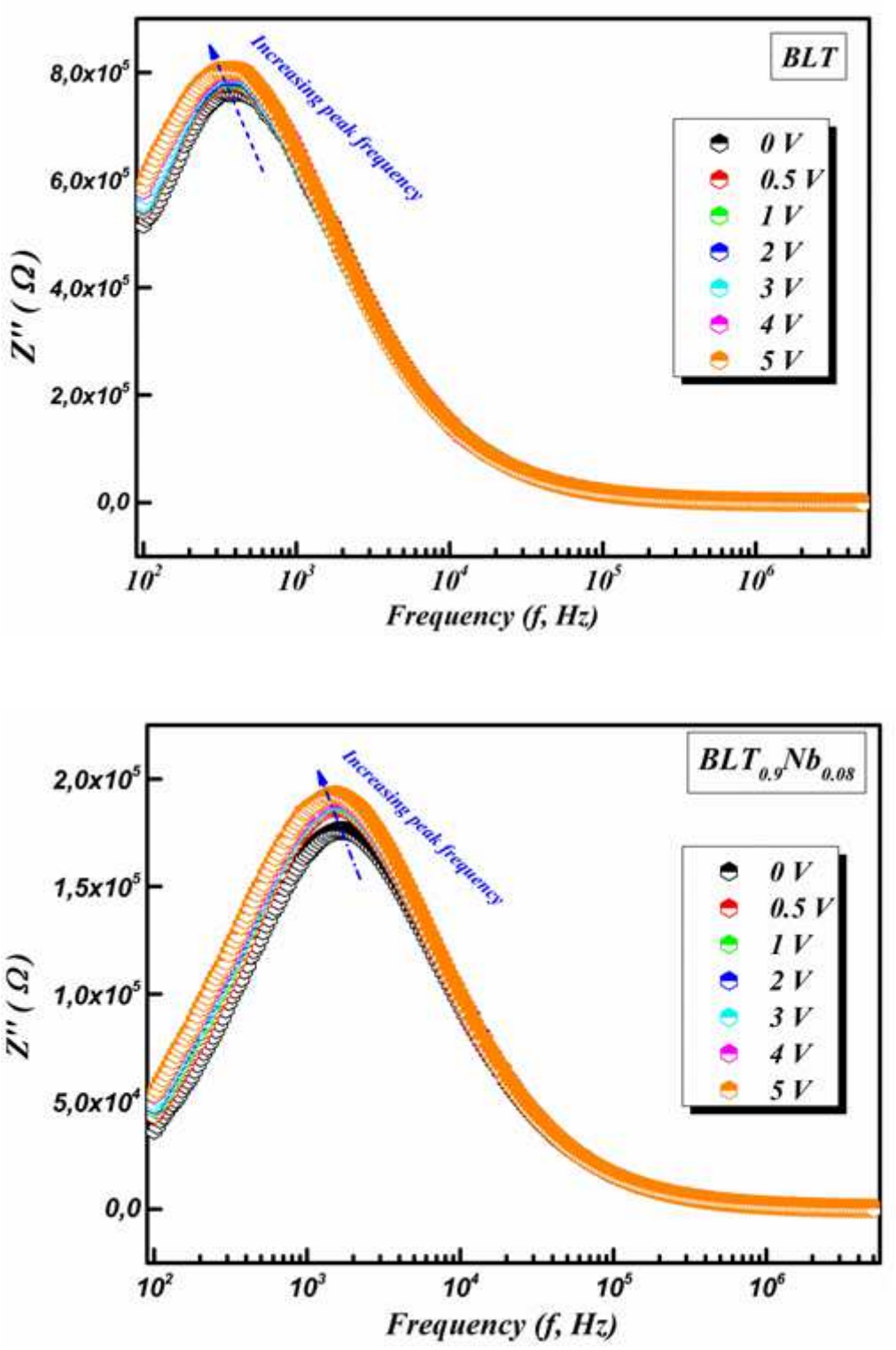


## Figure 4

Imaginary part of impedance as a function of DC-bias (V) for BLT and BLT0.9Nb0.08 ceramic samples

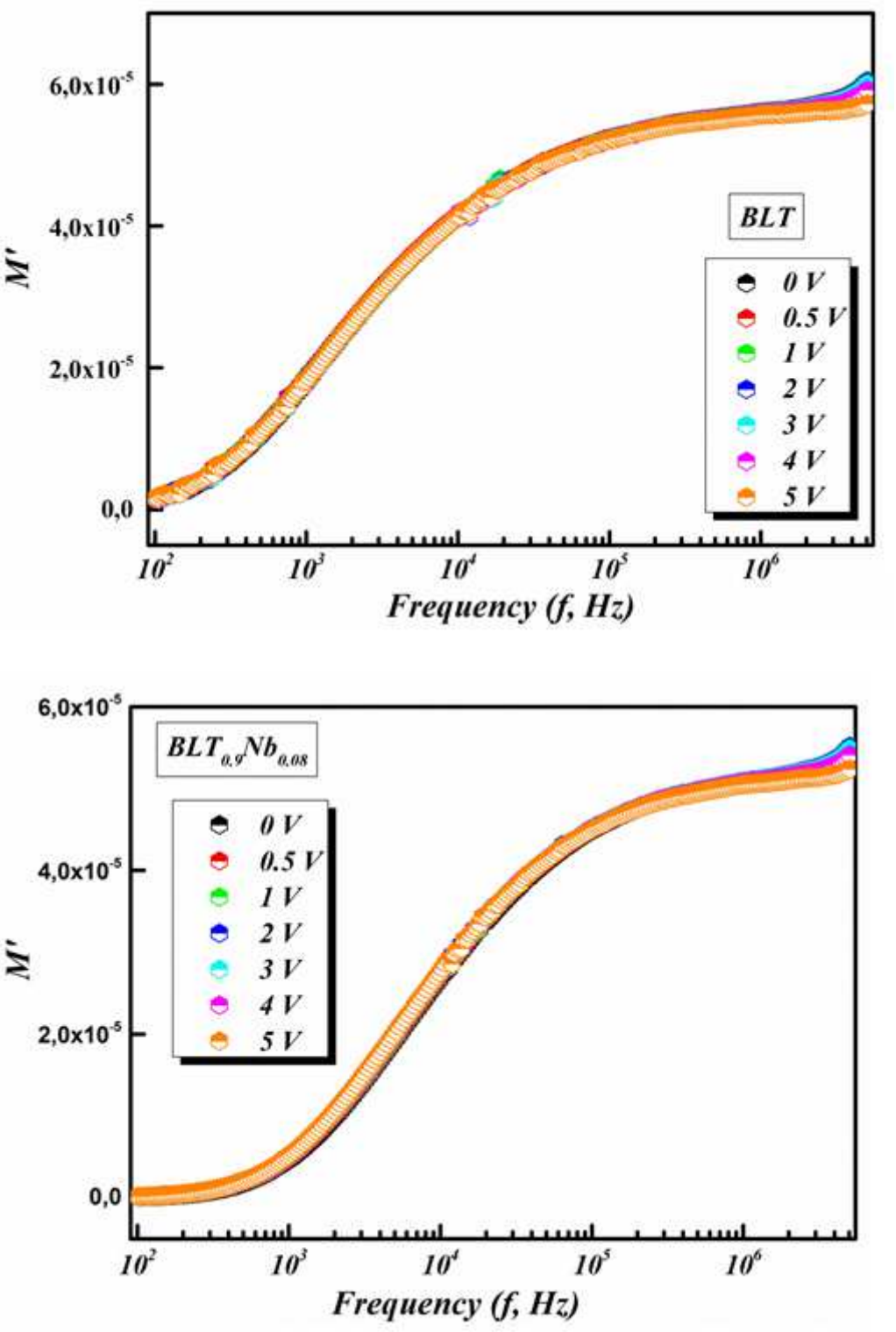


## Figure 5

Real modulus as a function of DC-bias (V) for BLT and BLT0.9Nb0.08 ceramic samples.

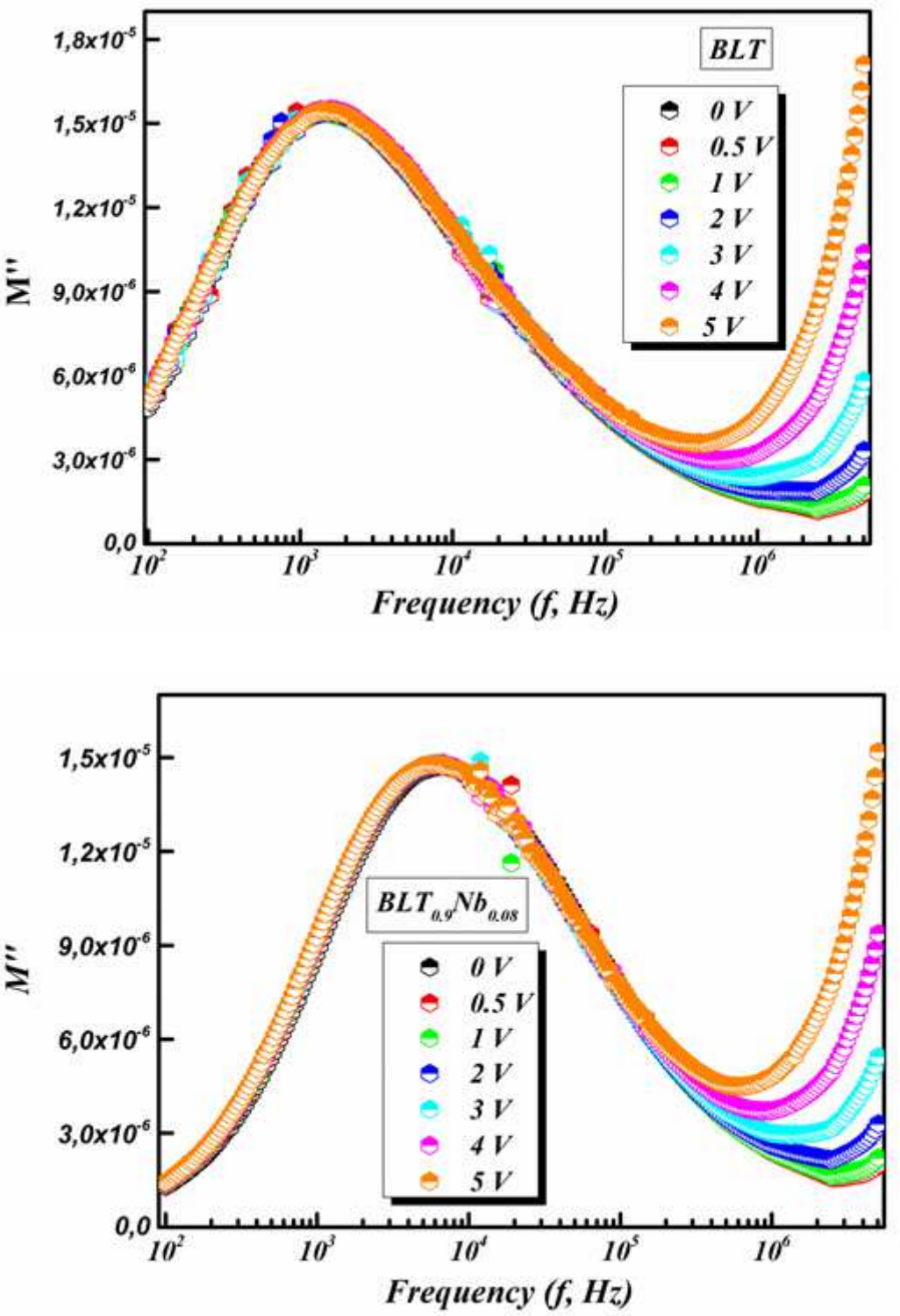


## Figure 6

Imaginary modulus as a function of DC-bias (V) for BT and BLT0.9Nb0.08 compounds.

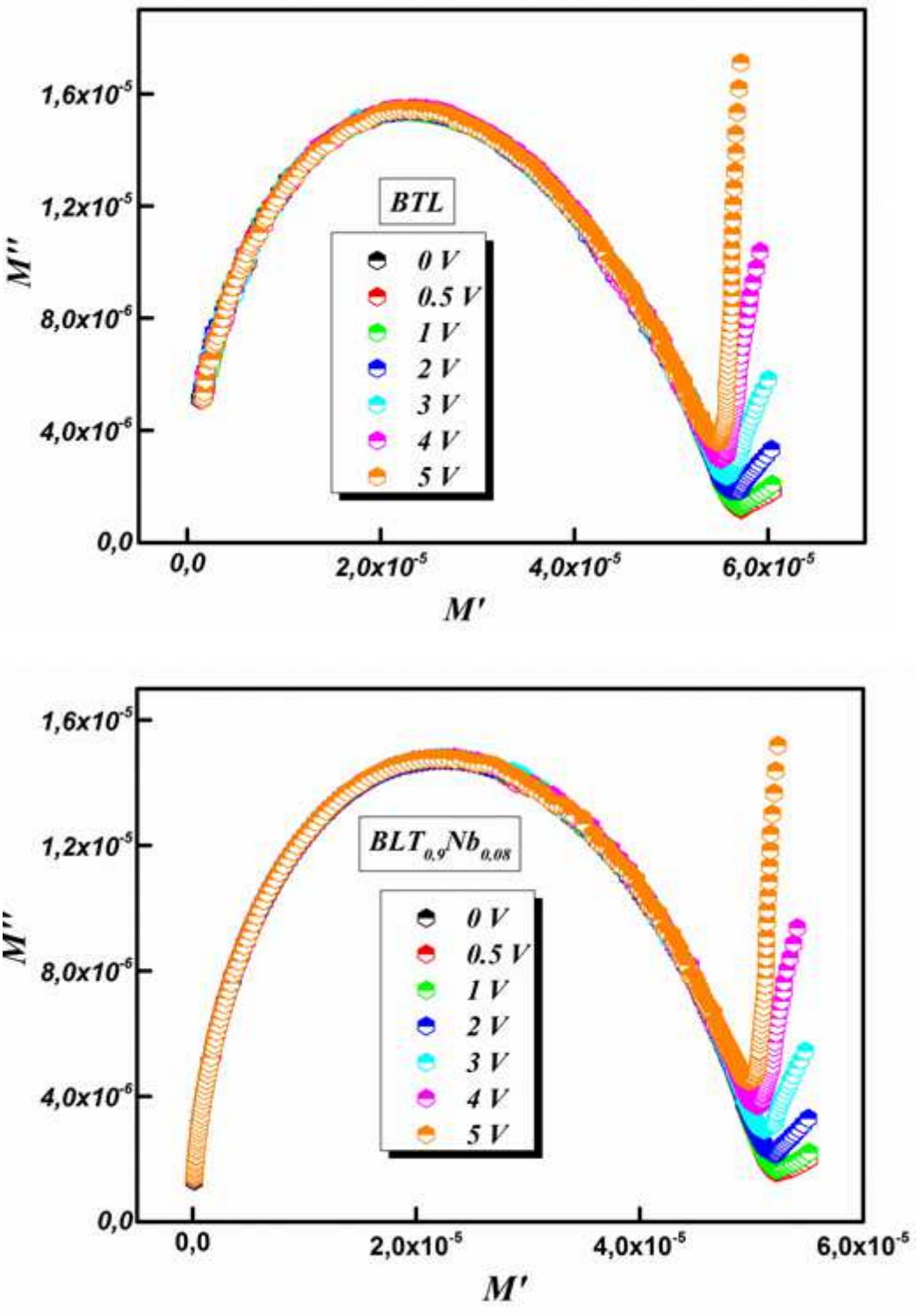


## Figure 7

Cole-Cole of modulus plots of BLT and BLT0.9Nb0.08 ceramic compounds under different DC bias.

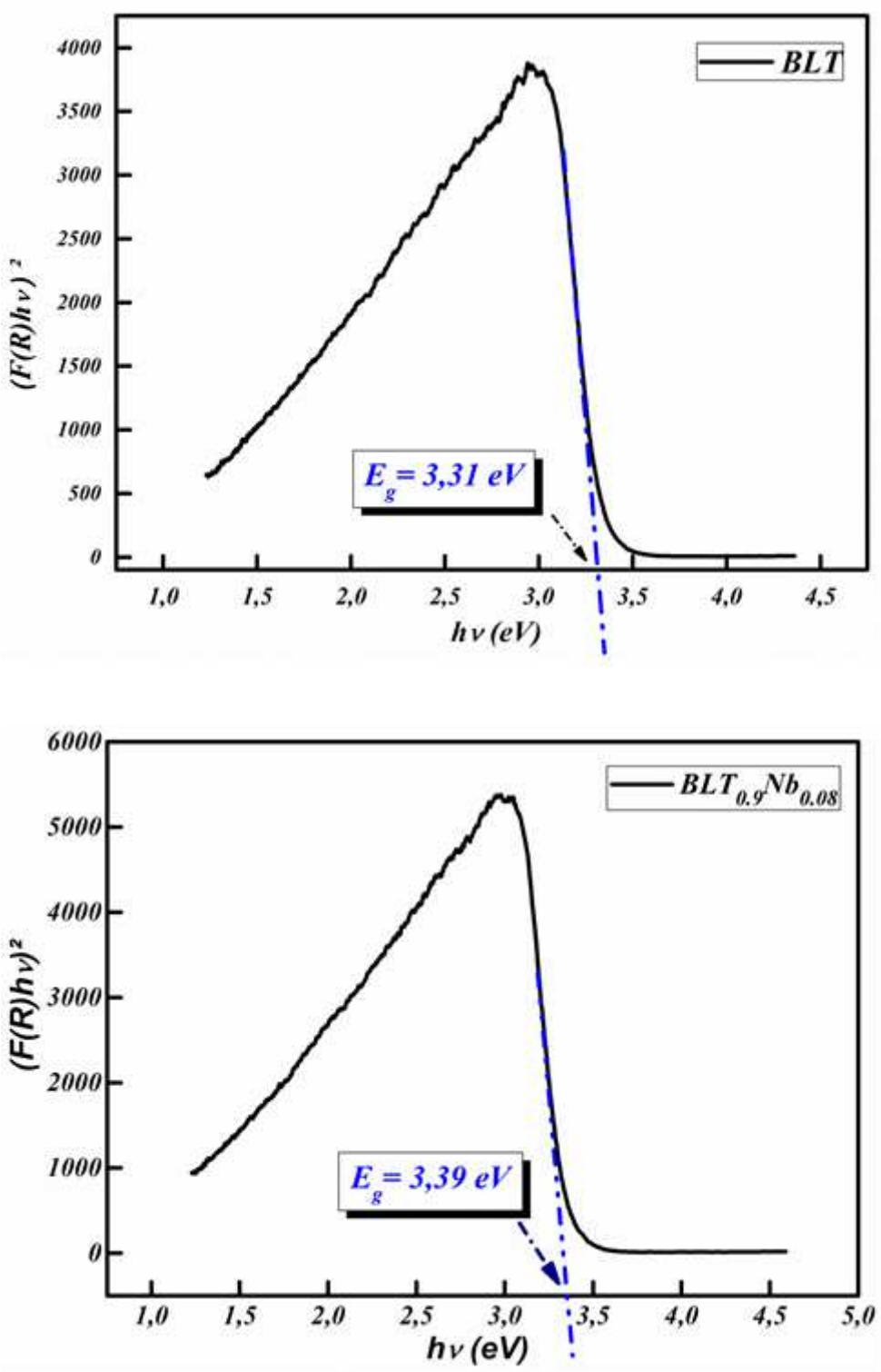


**Figure 8**

Kubelka-Munk plot of reflectance spectra to calculate the energy band gap of undoped and Nb5+ doped BLT ceramics.

## Supplementary Files

This is a list of supplementary files associated with this preprint. Click to download.

- Tablecaption.docx